HHS Public Access

Author manuscript

Phys Med Biol. Author manuscript; available in PMC 2017 September 07.

Published in final edited form as:

Phys Med Biol. 2016 September 07; 61(17): 6297–6306. doi:10.1088/0031-9155/61/17/6297.

A novel EPID design for enhanced contrast and detective quantum efficiency

Joerg Rottmann[1], **Daniel Morf**[2], **Rony Fueglistaller**[2], **George Zentai**[3], **Josh Star-Lack**[3], and **Ross Berbeco**[1]

[1]Brigham and Women's Hospital, Dana-Farber Cancer Institute and Harvard Medical School, Boston, USA [2]Varian Medical Systems, Baden, Switzerland [3]Varian Medical Systems, Palo Alto, USA

Abstract

Purpose—Beams-eye-view imaging applications such as real-time soft-tissue motion estimation are hindered by the inherently low image contrast of electronic portal imaging devices (EPID) currently available for clinical use. We introduce and characterize a novel EPID design that provides substantially increased detective quantum efficiency (DQE), contrast-to-noise ratio (CNR) and sensitivity without degradation in spatial resolution.

Methods—The prototype design features a stack of four conventional EPID layers combined with low noise integrated readout electronics. Each layer consists of a copper plate, a scintillator (GdO_2S_2: Tb) and a photodiode/TFT-switch (aSi:H). We characterize the prototype's signal response to a 6 MV photon beam in terms of modulation transfer function (MTF), DQE and contrast-to-noise ratio (CNR). The presampled MTF is estimated using a slanted slit technique, the DQE is calculated from measured normalized noise power spectra (nNPS) and the MTF and CNR is estimated using a Las Vegas contrast phantom. The prototype has been designed and built to be interchangeable with the current clinical EPID on the Varian TrueBeam platform (AS-1200) in terms of size and data output specifications. Performance evaluation is conducted in absolute values as well as in relative terms using the Varian AS-1200 EPID as a reference detector.

Results—A fivefold increase of DQE(0) to about 6.7% was observed by using the four-layered design versus the AS-1200 reference detector. No substantial differences are observed between each layer's individual MTF and the one for all four layers operating combined indicating that defocusing due to beam divergence is negligible. Also, using four layers instead of one increases the signal to noise ratio (SNR) by a factor of 1.7.

Conclusions—A layered EPID design improves the radiation sensitivity while maintaining the spatial resolution and saturation level of a single layer conventional EPID. Experimental characterization of this first 4-layered prototype demonstrates substantially improved DQE and CNR while maintaining a high resolution. Besides overall improved image quality and dosimetric sensitivity, we anticipate that this novel detector design will enable more accurate soft-tissue motion estimations during radiation therapy procedures.

Keywords

EPID; portal image; beams-eye-view; radiotherapy

1. Introduction

The beams-eye-view perspective of the patient's anatomy is particularly well suited for image guided radiotherapy (IGRT). Applications include the assessment of patient setup before and during treatment delivery as well as advanced motion assessment techniques such as markerless tumor tracking (Herman et al. (2001); Rottmann et al. (2013a,b)). Electronic portal imaging devices (EPID) can capture and display the fluence of the treatment beam after traversing the patient in real-time. However, the inherently low detective quantum efficiency (DQE) of these detectors in the MV energy range used in radiotherapy is a limiting factor for their clinical applications.

Most of the EPIDs currently in clinical use rely on an indirect photon detection mechanism. A scintillation material, typically terbium doped gadolinium oxysulfide (Gd_2O_2S: Tb), is sandwiched between a metal sheet top layer of 1 mm copper and a pixelated array of photodiodes typically referred to as an active matrix flat panel imager (AMFPI) (Street et al. (1990); Antonuk et al. (1990); Munro and Bouius (1998)). The copper plate serves a dual purpose: it shields the detector from low energy scattered secondary radiation and functions as a buildup layer converting high energy photons into secondary electrons. The scintillation material converts these incident electrons (and photons) into low energy photons in the optical range [‡] that can be detected with higher efficiency in the underlying photodiode array. The photodiode array is based on hydrogen doped amorphous silicon (aSi:H) and incorporates a thin film transistor (TFT) for the pixel readout. This technology allows the cost effective construction of large pixelated arrays that are very resistant to radiation damage (Antonuk (2002)). However, these EPIDs typically only achieve a DQE(0) of about 1–2 % inclinically used MV photon beams (El-Mohri et al. (2001)). While increasing the thickness of the scintillation layer can generate more detectable photons, optical scattering within the scintillator imposes a limit on the attainable DQE gain.

Developing high DQE scintillators has been a very active research area over the past decade, particularly with respect to megavoltage cone beam computed tomography (MV - CBCT) applications which require the minimization of imaging dose per frame to the patient in order to be clinically accept able (Pouliot et al. (2005)). One approach to this issue is to employ thick (focused) pixelated scintillators (Sawant et al. (2005,?); Wang et al. (2008); El-Mohri et al. (2011); Liu et al. (2012); Star-Lack et al. (2015)). DQE(0) values of up to 20 % have been observed using this technique (Star-Lack et al. (2015)). Another method to improve DQE is to stack several detector layers on top of each other creating a multi-layer imager (MLI). This approach is expected to preserve field of view and spatial resolution with respect to the current generation of clinically used EPIDs while al lowing to increase the DQE substantially. The purpose of this study was to construct a first prototype MLI

[‡]typically green for terbium doping

device based on the Varian AS-1200 AMFPI and characterize its quantitative imaging performance.

2. Materials and Methods

The MLI prototype presented in this study was constructed from four conventional EPID detection layers, i.e. 4 × [copper sheet - scintillator - AMFPI] (cf. Figure 1). Integrated readout electronics were custom designed for low noise characteristics and a compact assembly fitting inside the imager cassette of the Varian AS-1200. The prototype utilizes the AS-1200 AMFPI as a light converter (photodiode array) and the standard imaging interface of the TrueBeam linear accelerator (LINAC) platform for image acquisition. This allows for direct comparison of the MLI to the LINAC-mounted (and clinically used) AS-1200 EPID (further on referred to as reference detector). The MLI features internal parallel readout and digitization of all layers (within the imager cassette). All user - selected layers are internally integrated in a two - step digital addition process. For instance to read all four layers out: first $L12 = (L1(i, j) + L2(i, j))$ and $L34(i, j) = (L3(i, j) + L4(i, j))$ are calculated (in parallel) and then summed up in a second step to $L1234(i, j) = (L12(i, j) + L34(i, j))$. Here we used the notation $Ln(i, j)$ to refer to the pixel value at position (i, j) in the n-th layer. $L1234(i, j)$ alone is transferred as a true 16bit signal from the imager cassette to the LINAC image ac quisition system via optical link cable. Digitization of the analog photo diode signal within the imager cassette is expected to minimize electronic noise. While all image corrections (pixel defect, off set, gain) can be applied directly through the image acquisition system, we chose to apply them offline for easier data acquisition and analysis. However, the current image read out implementation is limited to pixel corrections applied to the integrated signal (over all used layers).

Each individual layer is covered by a 1 mm copper sheet providing buildup and scatter shielding for each layer, respectively. The selected scintillation material $GdO_2S_2:Tb$ (PI-200 by Mitsubishi Chemicals Corp., Japan) is slightly thicker than the Lanex Fast B (Eastman Kodak, Rochester, NY) scintillator used in the reference detector (430 μm versus 290 μm) but has the same density. A slightly stronger signal and a slightly reduced MTF is expected due to the increased number of interactions and optical scatter, respectively. The MLI prototype and the reference detector each have an active area of 43 cm × 43 cm and a pixel pitch of 336 μm. A comparison of MLI and reference detector characteristics is given in table 1.

All measurements described in this paper were performed using the 6 MV photon beam of a Varian TrueBeam LINAC. It was calibrated to deliver 1 cGy per monitor unit (MU) in water at a source to surface distance (SSD) of 100 cm and a depth of d_{max} = 1.5 cm using a 10×10 cm^2 field size (in this pa per all field sizes are defined at the isocenter plane). The dose rate for all measurements was set to 400 MU/min (i.e. our clinical standard dose rate for non - stereo tactic treatments). The source to imager distance (SID) refers to the distance between the source and the surface of the MLI imager cassette - in de pen dent of which layer (combination) is to be read out. Two modes of readout are supported: continuous and radshot. In continuous mode, the readout is synchronized with the radiation beam pulses to avoid radiation hitting the detector during readout. The MLI hardware supports a maximum

frame rate of 25 Hz. All images in this study were acquired in radshot mode, i.e. the signal is simply integrated throughout the exposure and read out right after the beam turns off. To clear residual charges before each exposure an additional readout cycle is completed right before each exposure. To label image acquisitions with various layer combinations the following nomenclature will be used throughout this manuscript: L1 denotes an acquisition with only the layer closest to the x-ray source, L4 with only the layer furthest from the x-ray source and L1234 denotes an acquisition with all four layers combined. Acquisitions with the reference detector (AS-1200) will be referred to as REF.

2.1. Evaluation in terms of MTF, nNPS, DQE

Modulation Transfer Function (MTF)—The MTF of an imaging system is given by the absolute value of the Fourier transform of its impulse response. For this study a one dimensional impulse (line spread function) formed by imaging a thin slit is utilized. Both the horizontal and vertical pixel direction of the detector are analyzed separately with this procedure. To avoid influence of the pixel grid's limited sampling frequency, the slit is tilted about 1.5° relative to the pixel row (column) direction and a presampled line spread function (LSF) is constructed following the procedure outlined by Fujita et al. (1992). There have been numerous publications describing this technique in detail (e.g. Munro and Bouius (1998); Sawant et al. (2007)); therefore only a short summary shall be given here.

A pair of tungsten heavy alloy blocks ($\approx$ 12 cm × 7.7 cm × 18.7 cm) is used to form the slit. Precision shims are placed in each corner to separate the machined surface of the blocks by 100 μm. The slit setup is placed on a robotic treatment couch and positioned relative to the radiation source, such that the central axis of the radiation beam is aligned with the slit (Sawant et al. (2007)). Alignment is established in a two step process: first the radiation field is aligned to the slit using a bi-directional laser and then the slit is aligned with the central axis of the radiation beam by maximizing the measured signal transmitted throughout the slit under variation of vertical position and pitch of the treatment table (cf. Figure 1). The SID for MTF measurements was SID = 151.5 cm and SID = 153 cm for the MLI and the reference detector, respectively. The presampled MTF is measured for each layer individually as well as for all four layers combined. To optimize signal to noise ratio (SNR) for the LSF images the dose per frame was adjusted to about 70% saturation level (making electronic noise negligible) and 200 frames were averaged.

Noise Power Spectrum (nNPS)—There are two major sources of noise present in the final image: systemic noise originating from the light-sensor/readout electronics and noise inherent in the quantum nature of the incident photons. Noise not associated with the incident photons can be analyzed with dark fields, i.e. images acquired without incident x-ray radiation. Conversely noise characteristics predominantly governed by quantum noise may be analyzed with flood field images of exposures close to the saturation limit given that noise from the readout electronics can be considered small and independent of the signal strength (Munro and Bouius (1998)).

For the measurement of the nNPS, 250 flood fields were acquired at an SID of 180 cm using a 10×10 cm^2 field. Following the procedure outlined by the International Electrotechnical

Commission (2003) a central region of about 120 × 120 pixels was processed to calculate first a 2D nNPS which was then transformed into a 1D nNPS by averaging the first ten rows on either side of the zero frequency axis (though not including it). Exposure for the flood fields was adjusted to about 70% saturation level. To remove fixed pattern noise, frames were pair-wise subtracted from each other. The nNPS was calculated for each layer individually as well as for all layers combined. The reference detector was characterized with the same method.

Detective Quantum Efficiency—The detective quantum efficiency of a system is given by

$$\mathrm{DQE}(f)=\frac{|\mathrm{MTE}(f)|^2}{q\cdot \mathrm{nNPS}(f)} \quad (1)$$

Here f is the spatial frequency (in line-pairs/mm), $|MTF(f)|$ the absolute value of the modulation transfer function, $nNPS(f)$ the normalized noise power spectrum and q the average incident x-ray fluence on the detector surface. The average photon fluence for an SID of $r_{ref} = 100\ cm$ was derived from a Monte Carlo model simulating the specific LINAC configuration ($q_0 = 1.42 \times 10^{-7} mm^{-2}\ cGy^{-1}$) (Star-Lack et al. (2014)). To correct for the measurement geometry an inverse square correction was applied, i.e. $q=q_0 \cdot r_{\mathrm{ref}}^2/r^2$ (with SID = r). Since the absolute value of the measured DQE relies on the accurate simulation of the average photon fluence q, we also calculated the relative performance of the MLI compared to the reference detector, the clinically used Varian AS-1200 EPID.

Linearity—The linearity of the detector prototype is an important characteristic of imaging performance as well as for transit dosimetry applications. The signal response was measured over the entire dynamic range for one layer (L1) as well as for all four layers combined (L1234) and compared to the reference detector (REF). Images were acquired using a 15×15 cm^2 field size and an SID of 140 cm. For each dose level several frames were acquired. Dose was measured using the recorded MU exposure in the image header and response was calculated as the average pixel value of a central 200 × 200 pixel area. No pixel corrections of any kind were applied. The maximum dose levels used were: 1.75MU, 7MU and 10MU for L1234, L1 and REF, respectively.

Las Vegas Contrast Phantom—We evaluated the imaging performance in terms of contrast to noise ratio (CNR) using a Las Vegas contrast phantom (Varian Medical Systems, Palo Alto, CA) as described by Herman et al. (2001). The phantom was setup isocentric with an SID of 150 cm. Each image was acquired with an exposure of 1 MU. The phantom consists of an aluminum plate with drilled holes of various diameters and depths. We used one of the holes (marked in Figure 5) to determine the CNR and evaluated visibility of the column with the smallest holes. For the evaluation of CNR a circular region of interest within the hole and a donut shaped region surrounding the hole was selected for the calculation of signal and background, respectively. CNR and SNR are given by:

$$\mathrm{CNR}=\frac{S_{in}-S_{\mathrm{out}}}{\sigma},\ \ \mathrm{SNR}=\frac{S}{\sigma_S} \quad (2)$$

Here S_{in} is the the mean signal of the circular ROI, S_{out} the mean signal of the donut shaped ROI and σ the image noise. S denotes the mean signal within the ROI and a the standard deviation of the background signal.

3. Results

A comparison of the horizontal versus vertical MTF, nNPS and DQE measurements confirmed good agreement in both directions (cf. Figure 2). We therefore only show the horizontal direction for all measurement results. Figure 3 shows the horizontal MTF of the MLI prototype detector for each layer individually, for all layers combined and for the Varian AS-1200 detector. The MTFs of the individual MLI layers are very similar, slightly degrading from L1 through L4. The combined MTF of all layers (L1234) is lower than the individual contributions. The benchmark MTF of the reference detector is higher in the mid-frequency range than the individual layers of the MLI, presumably due to the thinner scintillator (cf. also discussion).

The four layers of the MLI (L1,L2,L3,L4) show a similar noise characteristic over the entire frequency interval (cf. Figure 3, upper right). As expected, the reference detector collects more noise than each individual layer of the MLI. This is due to the use of a thicker scintillator in the MLI layers (higher photon yield). The combined layers L1234 have a much lower noise power spectrum than each MLI layer individually.

DQE as a function of spatial frequency is calculated from MTF and nNPS using equation (1) and the photon fluence. DQE(f) curves are plotted in Figure 3 (lower left) for each layer individually, for all layers combined and for the reference EPID detector. The DQE(f) relative to the reference detector is shown in Figure 3 (lower right.)

The dose linearity response is shown in Figure 4. Both MLI (L1 and L1234) as well as the reference detector display a linear response over the entire dynamic range. This compares well with previous findings for this type of detector (Munro and Bouius (1998)). Note that the absolute response value is different for L1 and L1234 by a factor of 4x due to the integration over four layers. The absolute response for the reference detector is lower due to the use of a thinner scintillator.

Images of the Las Vegas contrast phantom taken with L1, L12, L123, L1234 are shown in the top portion of Figure 5. All images were offset and gain corrected. Note the visibility of the left column and top row of circles as well as the increasing smoothness of the images from left to right. Quantitative measures of CNR and SNR (also for each single layer individually) are shown in the bottom part of Figure 5. The CNR and SNR enhancement ratios compute to: $\mathrm{CNR}_{L1234}/\mathrm{CNR}_{L1} = 1.6$ and $\mathrm{SNR}_{L1234}/\mathrm{SNR}_{L1} = 1.7$.

4. Discussion

In this study a novel multi-layer EPID design was presented. A first prototype with four copper-scintillator-AMFPI detection layers was built and its performance characterized and compared against the Varian AS-1200, the current standard EPID shipped with TrueBeam linear accelerators (Varian Medical Systems, Palo Alto, CA). Using a 6 MV photon beam, a DQE(0) of about 6.7% was measured with the MLI prototype. This constitutes an approximate 3–6x increase compared to EPIDs typically in clinical use today (Munro and Bouius (1998); Antonuk (2002)) and a fivefold increase compared to the AS-1200 used as a reference in this study. The increase in DQE may be attributed to the effect of both stacking multiple detection layers as well as increasing the thickness of the scintillator (relative to the reference EPID). The latter effect however also increases the optical spread within the scintillator, reducing the per layer MTF and overall DQE (cf. Figure 3) and thus limits the benefit of a thicker scintillator. Another effect, typically seen with thick scintillators, is defocusing due to beam divergence which would manifest as a degradation in MTF when comparing single layers to combined layers. While this may potentially become an issue in the MLI design if more (or thicker) layers were used, we did not observe degradation in MTF going from one layer to four layers. Furthermore it should be possible to correct for this effect since each layer could be pre-processed before integration. In the current implementation no particular attention was paid to pixel alignment which may have reduced the MTF combined layers. However, subpixel shifts may also al low CBCT resolution improvements (cf. Yoneyama et al. (2015)) which we will investigate in a future study. Another potential limiting factor to image quality of the MLI prototype is the integrated readout which does (in its current implementation) not allow the application of image corrections (off set, gain, pixel defect) before image integration. We plan to remove this issue in a future implementation.

As already mentioned in the introduction, various studies have explored other methods of increasing DQE, including the use of thick pixelated, focused scintillators. The pixelation of the scintillation material limits the aforementioned increase of optical spread with increasing material thickness and aligning the scintillator pixels to the divergent beam can reduce the effect of defocusing (Sawant et al. (2005); Star-Lack et al. (2015)). While these techniques can generate substantially higher DQE values, construction of such scintillators is technically more demanding and may be limited to smaller detectors with slightly lower spatial resolution mainly geared at MV-CBCT applications. The MLI is designed for ease of clinical adaptation: it offers all the benefits of the current EPID generation such as high spatial resolution, linear response and high frame rates in synchronized continuous mode and fits into the form factor of the AS-1200. The MLI cassette weighs slightly more than the AS1200. We however do not expect this to limit gantry mounting or substantially increase gantry sag.

There are several clinical applications that are expected to particularly benefit from the increased DQE of the MLI design: markerless tumor tracking performance should improve with increased CNR and decreased motion blurring due to smaller integration times (Yip et al. (2014); Rottmann et al. (2013b)). Also, MV-CBCT and simultaneous kV/MV imaging for patient setup will benefit from lower required dose and higher image quality. In future

studies these application aspects will be investigated more in detail and the layer composition as well as the number of MLI layers will be optimized using Monte Carlo techniques. Introducing a layer of thick pixelated scintillation material may allow simultaneous enhancement of planar and volumetric (CBCT) imaging capabilities.

5. Conclusions

The first prototype of a novel multi-layered EPID design for portal imaging and dosimetry was presented. The MLI improves the radiation sensitivity while maintaining the spatial resolution and saturation level of a single layer conventional EPID. Experimental characterization of an MLI prototype with four layers demonstrates substantially improved DQE and CNR while maintaining a high resolution comparable to clinically used EPIDs.

Acknowledgments

The project described was supported, in part, by Award Number R01CA188446-01 from the National Cancer Institute. The content is solely the responsibility of the authors and does not necessarily represent the official views of the National Cancer Institute or the National Institutes of Health.

References

Antonuk LE. Electronic portal imaging devices: a review and historical perspective of contemporary technologies and research. Phys Med Biol. 2002; 47(6):R31–R65. URL: http://dx.doi.org/10.1088/0031-9155/47/6/201. [PubMed: 11936185]

Antonuk L, Yorkston J, Boudry J, Longo M, Jimenez J, Street R. Development of hydrogenated amorphous silicon sensors for high energy photon radiotherapy imaging, IEEE Transactions on Nuclear Science. 1990; 37(2):165–170. URL: http://ieeexplore.ieee.org/stamp/stamp.jsp?arnumber=106612.

El-Mohri Y, Antonuk LE, Zhao Q, Choroszucha RB, Jiang H, Liu L. Low-dose megavoltage cone-beam ct imaging using thick, segmented scintillators. Phys Med Biol. 2011; 56(6):1509–1527. MLIpaper1, addon. URL: http://dx.doi.org/10.1088/0031-9155/56/6/001. [PubMed: 21325709]

El-Mohri Y, Jee KW, Antonuk LE, Maolinbay M, Zhao Q. Determination of the detective quantum efficiency of a prototype, megavoltage indirect detection, active matrix flat-panel imager. Med Phys. 2001; 28(12):2538–2550. URL: http://dx.doi.org/10.1118/1.1413516. [PubMed: 11797959]

Fujita H, Tsai DY, Itoh T, Doi K, Morishita J, Ueda K, Ohtsuka A. A simple method for determining the modulation transfer function in digital radiography. IEEE Trans Med Imaging. 1992; 11(1):34–39. URL: http://dx.doi.org/10.1109/42.126908. [PubMed: 18218354]

Herman MG, Balter JM, Jaffray DA, McGee KP, Munro P, Shalev S, Van Herk M, Wong JW. Clinical use of electronic portal imaging: report of aapm radiation therapy committee task group 58. Med Phys. 2001; 28(5):712–737. URL: http://dx.doi.org/10.1118/1.1368128. [PubMed: 11393467]

International Electrotechnical Commission. Medical electrical equipment—characteristics of digital x-ray imaging devices—part 1: determination of the detective quantum efficiency. 2003. URL: https://webstore.iec.ch/publication/21937

Liu L, Antonuk LE, Zhao Q, El-Mohri Y, Jiang H. Countering beam divergence effects with focused segmented scintillators for high dqe mega-voltage active matrix imagers. Phys Med Biol. 2012; 57(16):5343–5358. URL: http://dx.doi.org/10.1088/0031-9155/57/16/5343. [PubMed: 22854009]

Munro P, Bouius DC. X-ray quantum limited portal imaging using amorphous silicon flat-panel arrays. Med Phys. 1998; 25(5):689–702. URL: http://dx.doi.org/10.1118/1.598252. [PubMed: 9608480]

Pouliot J, Bani-Hashemi A, Chen J, Svatos M, Ghelmansarai F, Mitschke M, Aubin M, Xia P, Morin O, Bucci K 3rd, Roach M, Hernandez P, Zheng Z, Hristov D, Verhey L. Low-dose megavoltage cone-beam ct for radiation therapy. Int J Radiat Oncol Biol Phys. 2005; 61(2):552–560. URL: http://dx.doi.org/10.1016/j.ijrobp.2004.10.011. [PubMed: 15736320]

Rottmann J, Keall P, Berbeco R. Markerless epid image guided dynamic multi-leaf collimator tracking for lung tumors. Phys Med Biol. 2013a; 58(12):4195–4204. URL: http://dx.doi.org/10.1088/0031-9155/58/12/4195. [PubMed: 23715431]

Rottmann J, Keall P, Berbeco R. Real-time soft tissue motion estimation for lung tumors during radiotherapy delivery. Medical Physics. 2013b; 40(9):091713. URL: http://dx.doi.org/10.1118/1.4818655. [PubMed: 24007146]

Sawant A, Antonuk LE, El-Mohri Y, Li Y, Su Z, Wang Y, Yamamoto J, Zhao Q, Du H, Daniel J, Street R. Segmented phosphors: Mems-based high quantum efficiency detectors for megavoltage x-ray imaging. Med Phys. 2005; 32(2):553–565. URL: http://dx.doi.org/10.1118/1.1854774. [PubMed: 15789602]

Sawant A, Antonuk LE, El-Mohri Y, Zhao Q, Li Y, Su Z, Wang Y, Yamamoto J, Du H, Cunningham I, Klugerman M, Shah K. Segmented crystalline scintillators: an initial investigation of high quantum efficiency detectors for megavoltage x-ray imaging. Med Phys. 2005; 32(10):3067–3083. URL: http://dx.doi.org/10.1118/1.2008407. [PubMed: 16279059]

Sawant A, Antonuk L, El-Mohri Y. Slit design for efficient and accurate mtf measurement at megavoltage x-ray energies. Med Phys. 2007; 34(5):1535–1545. URL: http://dx.doi.org/10.1118/1.2717405. [PubMed: 17555235]

Star-Lack J, Shedlock D, Swahn D, Humber D, Wang A, Hirsh H, Zentai G, Sawkey D, Kruger I, Sun M, Abel E, Virshup G, Shin M, Fahrig R. A piecewise-focused high dqe detector for mv imaging. Med Phys. 2015; 42(9):5084. URL: http://dx.doi.org/10.1118/1.4927786. [PubMed: 26328960]

Star-Lack J, Sun M, Meyer A, Morf D, Constantin D, Fahrig R, Abel E. Rapid monte carlo simulation of detector dqe(f). Med Phys. 2014; 41(3):031916. URL: http://dx.doi.org/10.1118/1.4865761. [PubMed: 24593734]

Street, R., Nelson, S., Antonuk, L., Perez Mendez, V. MRS Proceedings. Vol. 192. Cambridge Univ Press; 1990. Amorphous silicon sensor arrays for radiation imaging; p. 441URL: http://dx.doi.org/10.1557/PROC-192-441

Wang Y, Antonuk LE, El-Mohri Y, Zhao Q, Sawant A, Du H. Monte carlo investigations of megavoltage cone-beam ct using thick, segmented scintillating detectors for soft tissue visualization. Med Phys. 2008; 35(1):145–158. URL: http://dx.doi.org/10.1118/1.2818957. [PubMed: 18293571]

Yoneyama A, Baba R, Sumitani K, Hirai Y. Feasibility study of a high-spatial resolution x-ray computed tomography using sub-pixel shift method. Appl Phys Let. 2015; 106(8) URL: http://dx.doi.org/10.1063/1.4913615.

Yip S, Rottmann J, Berbeco R. The impact of cine epid image acquisition frame rate on markerless soft-tissue tracking. Med Phys. 2014; 41(6):061702. URL: http://dx.doi.org/10.1118/1.4873322. [PubMed: 24877797]

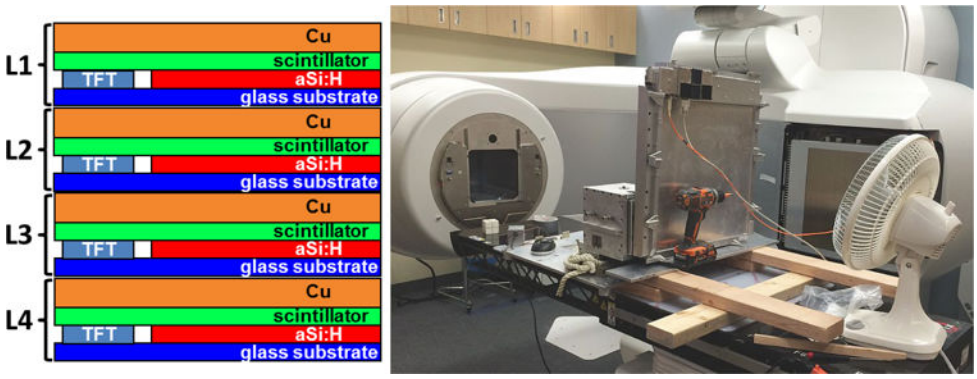

Figure 1.

(Left) Schematics of a single MLI pixel stack (not to scale) and data summation after digitization. The output is a by-pixel (digital) integration of all used layers. (Right) Setup for the MTF measurements with the MLI. The imager cassette is placed vertically on the couch. The aluminum box in front of the detector houses the set of jaws forming the slit. The orange fiber optic cable connects to the LINAC's image acquisition system (XI).

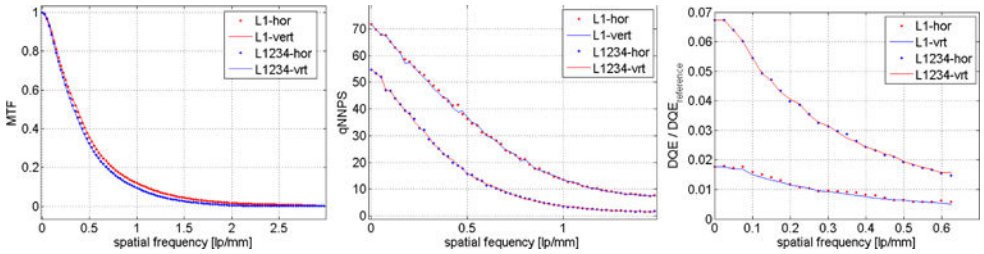

Figure 2.

Horizontal versus vertical measured parameters for L1 and L1234: (Left) presampled modulation transfer function, (Middle) normalized noise power spectrum, (Right) detective quantum efficiency.

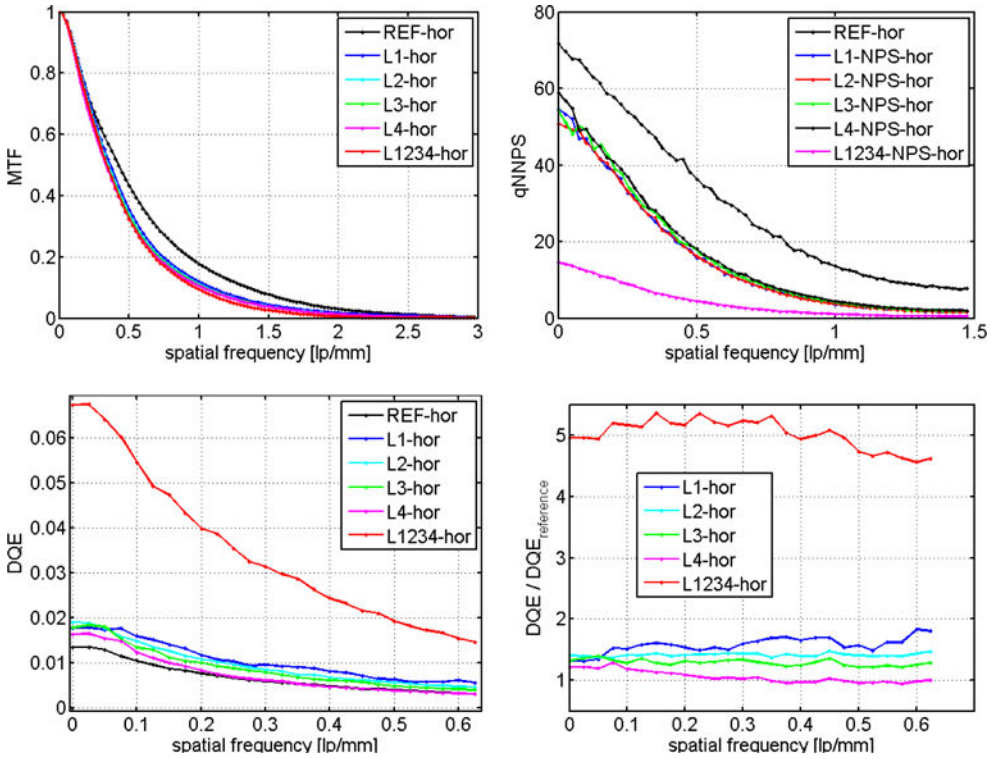

Figure 3.

(Left top) Presampled MTF measured with a slit (100 μm). (Top right) normalized noise power spectrum (MTF) calculated from flat field images (Bottom left) detective quantum efficiency (DQE) (Bottom right) DQE normalized by the value of the the Varian AS-1200 portal imager.

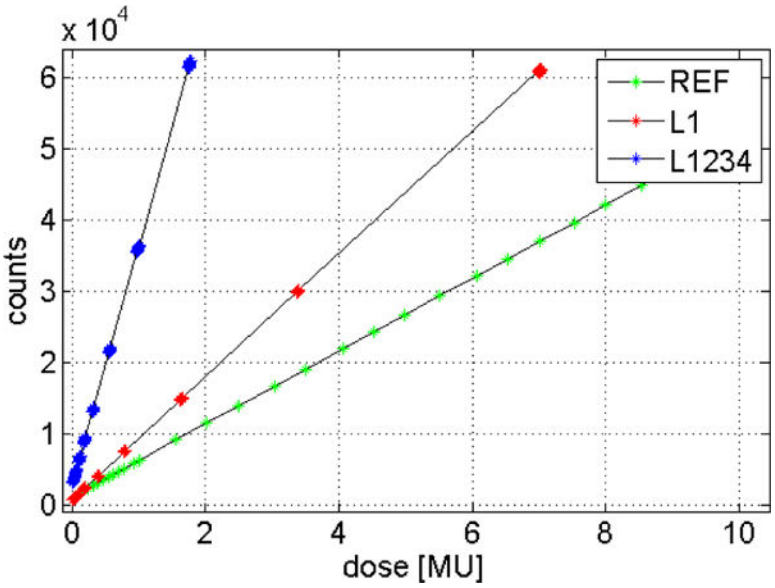

Figure 4.
Dose response linearity for the reference detector (AS-1200) and for the MLI layers L1 and L1234.

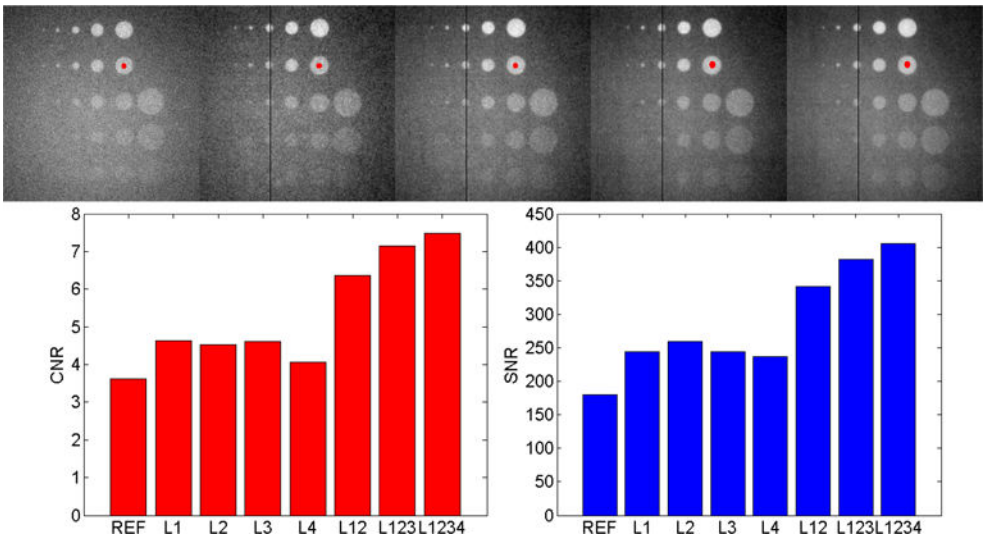

Figure 5.

(Top) Las Vegas contrast phantom for layer combinations (from left to right) REF, L1, L12, L123, L1234. The images are offset and gain corrected but not pixel defect corrected. The window/level was adjusted for best visibility. Notice the reduction in noise and increased visibility of the bottom circles from left to right. (Bottom) Contrast to noise ratio (CNR) and signal to noise ratio (SNR) for the reference detector, each MLI layer individually and all layer combinations.

Table 1

Comparison between the reference EPID (AS-1200) and the 4-layer MLI prototype. Both detectors utilize the same AMFPI as light detector.

	Reference (AS-1200)	**MLI prototype**
number of detector layers	1	4
metal sheet	1 mm copper	4 × 1 mm copper
scintillator	Lanex Fast B (290 μm)	4 × PI-200 (430 μm)
active area	43 cm × 43 cm	
pixel pitch	336 μm	
frame rate (synchronized mode)	10 Hz (maximum 25 Hz)	